Dual-Layer Optimization-Based Control Allocation for a Fixed-Wing UAV

Yunda Yan[a], Cunjia Liu[a,*], Hyondong Oh[b], Wen-Hua Chen[a]

[a]*Department of Aeronautical and Automotive Engineering, Loughborough University, Loughborough LE11 3TU, U.K.*

[b]*Department of Mechanical Engineering, Ulsan National Institute of Science and Technology (UNIST), Ulsan, South Korea*

Abstract

Many existing control allocation methods separate the high-level control design from their low-level allocation design, assuming that the constraints of actuators can be guaranteed by the allocator. This idea may not be suitable for the nonlinear fixed-wing unmanned aerial vehicle studied here, which hence motivates this work. In this paper, we propose a new dual-layer optimization-based control allocation method, in which the proposed allocator, on the one hand, can modify the pre-designed virtual signals from the high-level when the out-layer actuator, i.e., throttle, reaches its constraint. On the other hand, it reverts the conventional constrained allocator when the throttle constraints are inactive. Another feature is that under the proposed framework, the initial state of the augmented actuator dynamics serves as design parameters, bringing more degrees of freedom for allocation design without affecting the nominal stability. Apart from the control allocator, this paper also proposes a high-level flight controller based on the control-oriented model and a combination of nonlinear dynamic inversion and disturbance observer. Disturbance observer provides robustness by estimating the model errors between the control-oriented and true models, and compensating for them in the controller. High-fidelity simulation results under realistic wind disturbances are presented to demonstrate the performance of the proposed method.

Keywords: Flight control, disturbance observer, control allocation, actuator constraint, actuator dynamics.

*Corresponding author

Email addresses: y.yan3@lboro.ac.uk (Yunda Yan), c.liu5@lboro.ac.uk (Cunjia Liu), h.oh@unist.ac.kr (Hyondong Oh), w.chen@lboro.ac.uk (Wen-Hua Chen)

Nomenclature

h	altitude, [m]
V	airspeed, [m/s]
γ	flight path angle, [rad]
α	angle of attack, [rad]
q	pitch rate, [rad/s]
δ_T	throttle setting, [%/100]
δ_E	elevator deflection, [rad]
δ_F	flap deflection, [rad]
L	lift, [N]
D	drag, [N]
T	thrust, [N]
m	mass, [kg]
g	gravitational acceleration, [m/s^2]
J	moment of inertia, [kg·m^2]
ρ	density of air, [kg/m^3]
S	reference area, [m^2]
S_{prop}	propeller swiping area, [m^2]
C_{prop}	mean chord of the propeller
K_{motor}	motor constant
e	Oswald efficiency factor
AR	wing aspect ratio
c	mean aerodynamic chord of the wing
C_L	lift coefficient
$\bar{C}_L$	control-oriented lift coefficient
C_{L0}	C_L at zero angle of attack
C_L^α	variation of C_L w.r.t. the angle of attack
C_L^q	variation of C_L w.r.t. the pitch rate
$C_L^{\delta_E}$	variation of C_L w.r.t. the elevator
$C_L^{\delta_F}$	variation of C_L w.r.t. the flap
C_D	drag coefficient
$\bar{C}_D$	control-oriented drag coefficient
C_{D0}	minimum drag coefficient
$C_D^{\delta_E}$	variation of C_D w.r.t. the elevator
$C_D^{\delta_F}$	variation of C_D w.r.t. the flap
C_M	pitching moment coefficient
$\bar{C}_M$	control-oriented pitching moment coefficient
C_{M0}	C_M at zero angle of attack
C_M^α	variation of C_M w.r.t. the angle of attack
C_M^q	variation of C_M w.r.t. the pitch rate
$C_M^{\delta_E}$	variation of C_M w.r.t. the elevator
$C_M^{\delta_F}$	variation of C_M w.r.t. the flap

1. Introduction

Recent years have witnessed the explosive growth of applications of unmanned aerial vehicles (UAVs) in various domains, ranging from environment monitoring to cargo delivery. Among the different types of vehicles, fixed-wing UAVs, for example the Aerosonde aircraft, still stands out from the competition due to its multi-mission capability and world-class reliability [1]. On the one hand, a typical small fixed-wing aircraft is portable to deploy, low-cost to build, and flexible to operate [2]. On the other hand, they can be more easily equipped with multiple control surfaces, so as to meet the fault-tolerance requirement [3, 4, 5]. The over-actuation structure also has the potential to generate forces and moments in more extensive ranges to perform agile behavior or compensate for larger disturbances. This paper takes the Aerosonde aircraft, which equips with the throttle, (right and left) ailerons, flaps, and elevators as shown in Fig. 1, as an example to investigate usage of flaps as a control surface during the normal flight phase. This configuration, which may not be seen as common for small UAVs, is known as direct lift control in aviation and has the capability to improve the flight control performance, e.g., gust alleviation [6, 7].

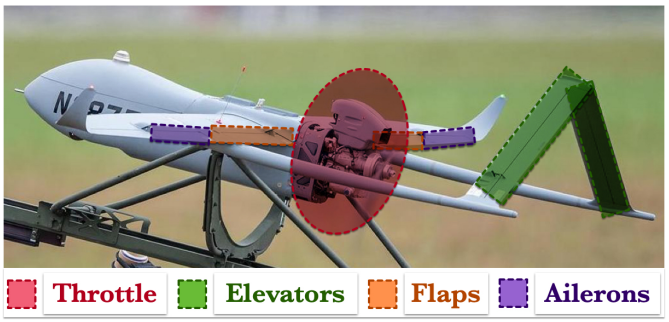

Figure 1: The control surfaces in Aerosonde.[1]

Contrary to its wide applications, the flight control design of Aerosonde has only attracted some attention in recent years, and most of the work is based upon classical methods, e.g., proportional-integral-derivative (PID) control [8, 9]. Another common approach is based upon the linearized model around specific equilibrium points and uses advanced strategies for different specifications,

[1]It is modified by the photograph from `https://www.textronsystems.com/products/aerosonde`. In this paper, only the longitudinal tracking control task is studied, and hence, the aileron control surfaces are ignored as they are usually applied in the lateral control; the flaps and elevators in the right and left are assumed to have the same behaviors for simplification.

e.g., fault-tolerant [5] and event-triggered [10] control methods. Although linearization of the aircraft dynamics yields well-known control analysis and design tools, such approaches are local in scope and cannot meet the requirements for a wider range of operational conditions. Gain schedule can relieve this problem by connecting multiple linear controllers [11], which however, inevitably brings more efforts on gain tuning. Generally, there is still room to improve the control performance if its nonlinearity is further exploited in the control design. However, the nonlinear control design for the Aerosonde aircraft is quite challenging due to the complex nonlinearities of the dynamics, e.g., intricate couplings among the motion dynamics, aerodynamics, and propeller thrust equation, leading to several complex expressions for the aerodynamic forces and moments. Another issue is the over-actuated dynamics. It can be seen that in the longitudinal tracking task, the throttle, flaps, and elevators all serve as control surfaces to control the altitude and velocity, and thus control allocation is required. In the early flight control studies of the Aerosonde aircraft [9, 10], however, the flaps are always set as zeros or the trim values, which implies that the redundant mechanical structure of the aircraft was not fully exploited.

The procedure of converting the control commands into individual actuators is referred to as the control allocation (see [12] for a detailed survey). Taking a general over-actuated system as an example, illustrated in Fig. 2, a high-level virtual controller $\boldsymbol{v}$ is assumed to be designed for tracking, whose dimension is the same as that of the regulated output or references; a low-level allocator is thus intended to distribute the desired control efforts generated by the virtual controller to the redundant physical actuators. The conventional control structure of a redundant system follows a hierarchical design goal of separating the high-level control from the low-level allocation [13, 14, 15], assuming that the safety of actuators could be guaranteed only by the allocator. Although the effectiveness has been proven by a large number of successful applications of the conventional allocation methods (e.g., daisy chaining and pseudoinverse), these approaches may not be suitable for the nonlinear fixed-wing aircraft studied in this paper. It will be shown later that the dynamic extension approach is required for the thrust dynamics to remove the non-minimum phase of the longitudinal model, which implies that the designed control signals (or, the allocated signals) are not physical anymore. Directly imposing constraints onto such virtual

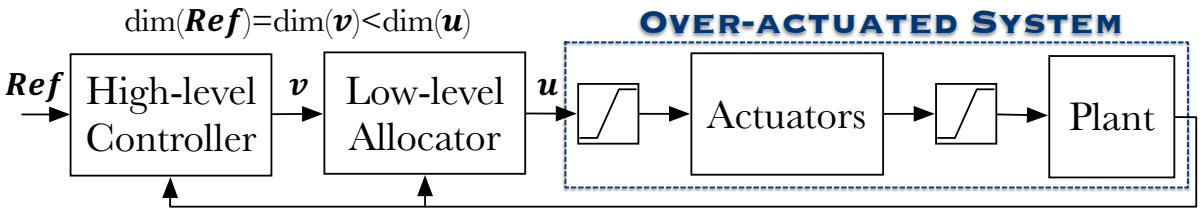

Figure 2: Control structure with the conventional control allocation.

signals does not mean the physical actuators would be within the constraints, and optimizing such virtual signals would lose the physical meaning in energy or economic saving.

The challenges as mentioned above are, at first glance, similar to the problems studied in another branch of allocation, with the name of *dynamic control allocation* [4, 7, 16, 17, 18, 19, 20, 21, 22, 23, 24], which emphasizes that the actuator dynamics are taken into consideration in the allocation design. However, the main difference is that the 'actuator dynamics' in the Aerosonde aircraft is artificially built to ensure that the relative degrees of the altitude and velocity are well defined. Such an artificial actuator brings more degrees of freedom for allocation design as the initial states of the actuator can be regarded as the design parameters. Although these two problems are essentially different, great inspiration and understanding could be brought from advanced dynamic allocation methods. Arguably, the first solution on the actuator dynamics in control allocation appears in [16] by punishing the allocation rates in the optimization process, which has also been developed into the closed-loop control allocation in [4, 17]. The drawback of this pioneering work is that the actuator model cannot be explicitly embedded into the allocation design, even if it is linear and known, which makes the offset-free allocation only be achieved when the high-level control signals are constant [16, Th. 3]. In [18], the lag effect of actuator dynamics is approximatively compensated by using the actuator states and their changing rates in the last sampling time. However, such a compensation method is not suitable here as precise discretization is almost impossible for the nonlinear dynamics of the considered UAV. In [19], a linear matrix inequality-based control allocation is proposed considering actuator dynamics and constraints on actuator position and rate; however, this requires solving the nontrivial optimization problem in real time. Following the model predictive control (MPC) framework, a new constrained control allocation scheme is proposed in [20, 21]. Due to the prediction feature of MPC, not only the

current actuator states but also future ones in the receding horizon should be involved in solving the constrained optimization problem, which would cause high computing resources. In [7], an explicit MPC-based dynamic allocator is proposed for the tracking problem of a linearized aircraft model driven by linear actuators without constraints. In [22], the output regulation problem for over-actuated linear systems is solved, which can be applied to the case of linear actuators but without constraints. In [23, 24], the optimality-based dynamic allocation is designed for redundancy actuators with the first-order nonlinear dynamics, where the actuator constraints are involved via suitable penalty terms in the cost function. However, similarly to the pioneering work [16], offset-free allocation can only be achieved in the case of constant control signals [24, Th. 1], which is not suitable for the highly maneuverable flight control. To conclude, it is still challenging for the control allocation design of the Aerosonde as it involves the strong nonlinear aircraft dynamics with the time-varying tracking task and the actuators with dynamics and physical constraints, which means that the aforementioned dynamic allocation methods for a linear plant or set-point tracking (stabilization) task are not directly applicable.

To solve the constrained allocation problem of the nonlinear aircraft dynamics, this paper proposes a new dynamic allocation method using dual-layer quadratic programming (QP). Before the detailed design, a nonlinear control-oriented model with well-defined relative degrees is first established by simplifying several parts of aerodynamics. Its applicability can be proved to sufficiently cover the normal operating range of the aircraft, whose properties are thoroughly exploited in both the control and allocation design. To pursuit the modular design, the actuator safety task is left to the low-level allocation while the basic tracking is covered by the high-level control. In this case, the high-level control design based on the nonlinear dynamic inversion (NDI) is not the main focus. Nevertheless, disturbance observers (DOs) [25] are used to estimate the model errors between the control-oriented model and the true model and compensate for such errors. Readers can refer to [26, 27, 28, 29, 30, 31] for the advantages of this composite approach in the flight control systems. In the low-level, by properly reconstructing the barrier function from [32], a dual-layer QP-based control allocator is proposed to relieve the conflict between tracking objectives and actuator constraints. The actuator dynamics and physical constraints are both explicitly

considered by the proposed allocator. Compared with the conventional allocation methods, the proposed approach has a more flexible structure as it can modify the high-level control commands and is compatible with the general nonlinear control methods adopted in the high level.

The remainder is organized as follows. The problem formulation is provided in Section 2. The control-oriented model and detailed NDI and DO design are all introduced in Section 3. The dual-layer QP-based allocation design is in Section 4. Simulations on the improvements of allocation and tracking are in Section 5. Section 6 concludes this paper.

Notation: Throughout this paper, vectors and matrices are written in the bold typestyle to avoid ambiguity. For any smooth enough function $f(t)$, symbol $f^{(i)}(t)$ denotes the i-th order derivative of $f(t)$ with respect to variable t. Symbol $\mathcal{L}_f\varphi$ denotes the Lie derivative of the function φ along the vector field f. Matrix $\boldsymbol{I}_{k\times k}$ denotes a $k \times k$ identity matrix and matrix $\mathbf{0}_{i\times j}$ denotes an $i \times j$ zero matrix.

2. Problem Formulation

2.1. Aerosonde Dynamics

Direct derivation based on Lagrange's equations can give the following equations of motion of the longitudinal dynamics for the general fixed-wing aircraft:

$$\begin{aligned}
\dot{h} &= V\sin\gamma \\
\dot{V} &= \frac{T\cos\alpha - D}{m} - g\sin\gamma \\
\dot{\gamma} &= \frac{T\sin\alpha + L}{mV} - \frac{g\cos\gamma}{V} \\
\dot{\alpha} &= q - \dot{\gamma} \\
\dot{q} &= \frac{M}{J}
\end{aligned} \tag{1}$$

where the associated forces and moments are generated by [2, Chap. 4]:

$$\begin{aligned} L &= \frac{1}{2}\rho V^2 S C_L \\ D &= \frac{1}{2}\rho V^2 S C_D \\ M &= \frac{1}{2}\rho V^2 S c C_M \\ T &= \frac{1}{2}\rho S_{\text{prop}} C_{\text{prop}} \left(K_{\text{motor}}^2 \delta_T^2 - V^2\right). \end{aligned} \tag{2}$$

The aerodynamic moment coefficients of the Aerosonde aircraft are expressed as nonlinear combinations of states and control inputs as follows [33, Chap. 4]:

$$\begin{aligned} C_L(\alpha, q, V, \delta_E, \delta_F) &= C_{L0} + C_L^{\alpha}\alpha + C_L^{q}\frac{c}{2V}q + C_L^{\delta_E}\delta_E + C_L^{\delta_F}\delta_F \\ C_D(\alpha, q, V, \delta_E, \delta_F) &= C_{D0} + \frac{(C_L - C_{L0})^2}{\pi e A R} + C_D^{\delta_E}\delta_E + C_D^{\delta_F}\delta_F \\ C_M(\alpha, q, V, \delta_E, \delta_F) &= C_{M0} + C_M^{\alpha}\alpha + C_M^{q}\frac{c}{2V}q + C_M^{\delta_E}\delta_E + C_M^{\delta_F}\delta_F. \end{aligned} \tag{3}$$

Letting $\boldsymbol{x} \triangleq [h,\ V,\ \gamma,\ \alpha,\ q]^T$ and $\boldsymbol{u} \triangleq [\delta_T,\ \delta_E,\ \delta_F]^T$, the original Aerosonde model (1)-(2)-(3) can be described by the following compact form:

$$\dot{\boldsymbol{x}} = \boldsymbol{F}(\boldsymbol{x}, \boldsymbol{u}) \tag{4}$$

which is non-affine due to the complex dynamics of propeller thrust equation in (2) and couplings between the lift and drag coefficients in (3). By continuously differentiating system outputs $\boldsymbol{y} \triangleq [h,\ V]^T$, $\boldsymbol{u}$ firstly appears in $h^{(2)}$ and $V^{(1)}$, respectively, implying that the relative degrees of outputs are not well defined and the zero dynamics exists.

2.2. Control Objective

The objective of this paper is to design three control inputs, δ_T, δ_E, and δ_F, such that the outputs of the Aerosonde aircraft, h and V, asymptotically track the given references, h_r and V_r, as closely as possible. Meanwhile, the designed control inputs are required to be within their physical constraints for safety. Generally, the throttle should be in $(0, 100\%]$, and both the elevator and flap should usually be in $[-60°, 60°]$, or in smaller constraint sets. It is worth noting that,

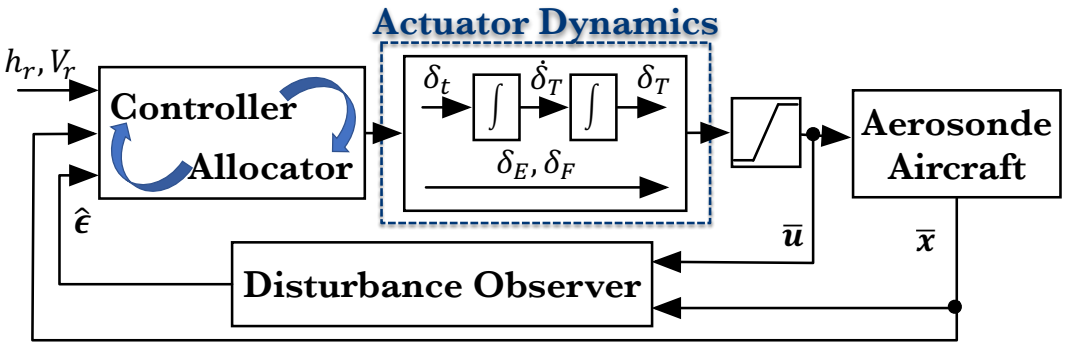

Figure 3: Schematic diagram of the proposed method.

from the practical point of view, safety is the higher priority goal than tracking performance. Before the detailed control and allocation design, the schematic diagram of the proposed method is first presented in Fig. 3, where the proposed tracking controller in the high level and constrained allocator in the low level will be followed later by Figs. 4 and 5, respectively.

3. Control Design

3.1. Control-Oriented Modeling

As mentioned briefly in the preceding section, strong non-minimum phase nonlinearities exist in the model (4). Theoretically, as observed from (3), the non-minimum phase behavior stems from the coupling of the elevator and flap to the lift and drag forces. A possible solution is to build a control-oriented model by ignoring the weak elevator and flap couplings [34], as represented by the following aerodynamic moment coefficients:

$$\begin{aligned} \bar{C}_L(\alpha) &\triangleq C_{L0} + C_L^{\alpha}\alpha \\ \bar{C}_D(\alpha) &\triangleq C_{D0} + \frac{\left(\bar{C}_L - C_{L0}\right)^2}{\pi e AR} \\ \bar{C}_M(\alpha, \delta_E, \delta_F) &\triangleq C_{M0} + C_M^{\alpha}\alpha + C_M^{\delta_E}\delta_E + C_M^{\delta_F}\delta_F. \end{aligned} \tag{5}$$

To facilitate the control design of NDI [35, Chap. 5.4], a second-order actuator model is introduced for the throttle, i.e., $\ddot{\delta}_T = \delta_t$, which is intended to confirm that the output vector has well-defined relative degree with respect to the new input. Letting $\bar{\boldsymbol{x}} \triangleq \left[h,\ V,\ \gamma,\ \alpha,\ q,\ \delta_T,\ \dot{\delta}_T\right]^T$ and

$\bar{\boldsymbol{u}} \triangleq [\delta_t,\ \delta_E,\ \delta_F]^T$, the control-oriented model is given as follows:

$$\dot{\bar{\boldsymbol{x}}} = \boldsymbol{f}(\bar{\boldsymbol{x}}) + \boldsymbol{g}(\bar{\boldsymbol{x}})\bar{\boldsymbol{u}} \triangleq \bar{\boldsymbol{f}}(\bar{\boldsymbol{x}}, \bar{\boldsymbol{u}}) \tag{6}$$

where $\boldsymbol{f}(\bar{\boldsymbol{x}})$ and $\boldsymbol{g}(\bar{\boldsymbol{x}})$ are the system functions generated by the aerodynamic moment coefficients (5). It can be straightforward to check that the output of the control-oriented model (6) has full vector relative degree, allowing a normal form to be explicitly derived following [35, Chap. 5.6]. By using the appropriate change of coordinate, $\bar{\boldsymbol{z}} \triangleq \left[h,\ \mathcal{L}_{\boldsymbol{f}}h,\ \mathcal{L}^2_{\boldsymbol{f}}h,\ \mathcal{L}^3_{\boldsymbol{f}}h,\ V,\ \mathcal{L}_{\boldsymbol{f}}V,\ \mathcal{L}^2_{\boldsymbol{f}}V\right]^T = [\bar{z}_i]_{7\times 1}$, system (6) is then able to be rewritten in the normal form:

$$\begin{gathered} \dot{\bar{z}}_i = \bar{z}_{i+1},\ i = 1, 2, 3, 5, 6 \\ \begin{bmatrix} \dot{\bar{z}}_4 \\ \dot{\bar{z}}_7 \end{bmatrix} = \begin{bmatrix} \mathcal{L}^4_{\boldsymbol{f}}h \\ \mathcal{L}^3_{\boldsymbol{f}}V \end{bmatrix} + \begin{bmatrix} \mathcal{L}_{\boldsymbol{g}}\mathcal{L}^3_{\boldsymbol{f}}h \\ \mathcal{L}_{\boldsymbol{g}}\mathcal{L}^2_{\boldsymbol{f}}V \end{bmatrix} \bar{\boldsymbol{u}} \end{gathered} \tag{7}$$

where the control gain matrix of (7) can be denoted as

$$\boldsymbol{B}(\bar{\boldsymbol{x}}) = [b_{ij}(\bar{\boldsymbol{x}})]_{2\times 3} \triangleq \begin{bmatrix} \mathcal{L}_{\boldsymbol{g}}\mathcal{L}^3_{\boldsymbol{f}}h \\ \mathcal{L}_{\boldsymbol{g}}\mathcal{L}^2_{\boldsymbol{f}}V \end{bmatrix} \tag{8}$$

whose elements are represented in Appendix A. From (7), the whole nonlinear system has been divided into two independent subsystems: the altitude and velocity subsystems.

Before a detailed control design, it is necessary to fully explore the propositions of the proposed control-oriented model (7). Note that the longitudinal flight control task is required to control the altitude h and velocity V, separately, which implies that the system (7) should have two degrees of freedom over its operating range of interest. Such a requirement is equivalent to the rank condition, i.e., $\text{rank}(\boldsymbol{B}(\bar{\boldsymbol{x}})) = 2$. Actually, similar requirements are embedded in many NDI-based aerospace literature [26, 27, 28, 34, 36, 37], i.e., $\boldsymbol{B}(\bar{\boldsymbol{x}})$ is non-singular, although these works are not for the over-actuated aircraft. In the following lemma, we will give a more explicit condition on the system states of (7) to show when the rank condition can be satisfied.

Lemma 1. *Consider the control-oriented system (7). If the following inequalities hold:*

$$V > 0,\ \delta_T > 0,\ \gamma \in (-\pi/2, \pi/2),\ \Gamma(\alpha) \geq 0$$

where $\Gamma(\alpha) \triangleq 2SC_L^{\alpha 2} \cdot \alpha \sin(\alpha) + \pi eARSC_L^{\alpha} \cdot \cos(\alpha) - \pi eARC_{prop}S_{prop}$*, then rank*$(\boldsymbol{B}(\bar{\boldsymbol{x}})) = 2$*.*

Proof. For conciseness, the following two propositions are given, which are also significant in the control and allocation design subsequently. Proposition 1 is first obtained from the direct calculation of the elements in Eq. (8). Based upon Proposition 1, Proposition 2 holds as the rank of a matrix is the maximal number of linearly independent columns.

Proposition 1. $\forall \bar{\boldsymbol{x}} \in \mathbb{R}^7,\ b_{12}(\bar{\boldsymbol{x}})b_{23}(\bar{\boldsymbol{x}}) - b_{13}(\bar{\boldsymbol{x}})b_{22}(\bar{\boldsymbol{x}}) = 0.$

Proposition 2. *rank*$(\boldsymbol{B}(\bar{\boldsymbol{x}})) = 2$*, if and only if* $b_{11}(\bar{\boldsymbol{x}})b_{22}(\bar{\boldsymbol{x}}) - b_{12}(\bar{\boldsymbol{x}})b_{21}(\bar{\boldsymbol{x}}) \neq 0.$

Using the alternative condition given in Proposition 2, we only need to calculate the following variable:

$$\begin{aligned} b_{11}(\bar{\boldsymbol{x}})b_{22}(\bar{\boldsymbol{x}}) - b_{12}(\bar{\boldsymbol{x}})b_{21}(\bar{\boldsymbol{x}}) = &- \frac{C_M^{\delta_E} C_{\text{prop}} K_{\text{motor}}^2 S S_{\text{prop}} c \rho^3}{4\pi eARJm^2} \cdot \delta_T \cos(\gamma) V^2 \\ &\cdot \left(V^2 \Gamma(\alpha) + \pi eARC_{\text{prop}} S_{\text{prop}} K_{\text{motor}}^2 \cdot \delta_T^2 \right). \end{aligned} \tag{9}$$

Keeping in mind the physical meanings of variables in the fixed-wing aircraft, a sufficient condition to render (9) nonzero is: $V > 0,\ \delta_T > 0,\ \gamma \in (-\pi/2, \pi/2),\ \Gamma(\alpha) \geq 0$, which hence completes the proof. ■

Considering the parameters of the Aerosonde aircraft in Appendix B, we will have $\Gamma(\alpha) = 1.3262\cos(\alpha) + 34.6267\alpha\sin(\alpha) - 0.0871$. It is also elementary to get that $\Gamma(\alpha) \geq \Gamma(0) = 1.2391$ holds for $\alpha \in (-\pi/2, \pi/2)$. This implies that the rank condition be further relaxed as:

$$V > 0,\ \delta_T > 0,\ \gamma, \alpha \in (-\pi/2, \pi/2),$$

which is generally satisfied if the considered Aerosonde aircraft is working on its normal condition. As a result, the rank condition will not be emphasized in the rest of this paper by assuming that

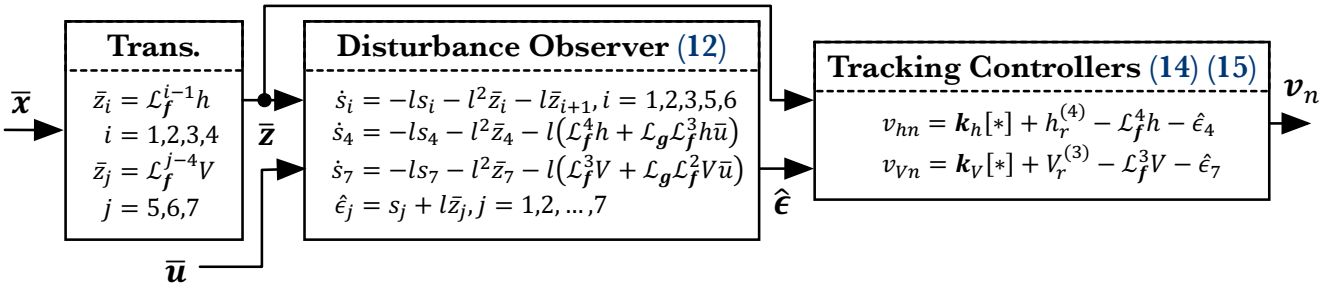

Figure 4: Schematic diagram of the proposed tracking controller in the high level.

$\text{rank}(\boldsymbol{B}(\bar{\boldsymbol{x}})) = 2$.

3.2. Dynamic Inversion and Uncertainties Compensation

Based on the normal form (7), it is straightforward to design the standard NDI controller, which works well for the control-oriented model (6). However, considering the model error between the true model (4) and the control-oriented one (6), compensation for such a model error is necessary for the high-precision tracking objective. This can be usually achieved by adding an integral on the tracking error [34, 36] or using a disturbance observer to estimate and compensate for the model error [26, 28, 38], while the latter one is adopted in this paper. Detailed comparison on these two approaches is beyond the scope of this paper; readers are directed to [26] for the thorough analysis. For easy understanding, the proposed controller is first illustrated by Fig. 4 with several key equations.

In the subsequent, a disturbed normal form of the true model (4) will be established. Under the same extension of the throttle, the original model (4) can be rewritten as follows:

$$\dot{\bar{\boldsymbol{x}}} = \bar{\boldsymbol{F}}(\bar{\boldsymbol{x}}, \bar{\boldsymbol{u}}). \tag{10}$$

Along system (10), state $\bar{\boldsymbol{z}}$ will be in a different dynamics:

$$\begin{aligned} \dot{\bar{z}}_i &= \bar{z}_{i+1} + \epsilon_i, \ \ i = 1,2,3,5,6 \\ \begin{bmatrix} \dot{\bar{z}}_4 \\ \dot{\bar{z}}_7 \end{bmatrix} &= \begin{bmatrix} \mathcal{L}_f^4 h \\ \mathcal{L}_f^3 V \end{bmatrix} + \begin{bmatrix} \epsilon_4 \\ \epsilon_7 \end{bmatrix} + \boldsymbol{B}(\bar{\boldsymbol{x}})\bar{\boldsymbol{u}} \end{aligned} \tag{11}$$

where $\epsilon_i \triangleq \mathcal{L}_{\bar{\boldsymbol{F}}-\bar{\boldsymbol{f}}}\mathcal{L}_{\bar{\boldsymbol{f}}}^{i-1}h,\ i=1,2,3,4$ and $\epsilon_j \triangleq \mathcal{L}_{\bar{\boldsymbol{F}}-\bar{\boldsymbol{f}}}\mathcal{L}_{\bar{\boldsymbol{f}}}^{j-5}V,\ j=5,6,7$. By regarding all the model errors ϵ_i $(i=1,2,\cdots,7)$ as unknown states, seven first-order linear DOs are designed to estimate the model errors, respectively:

$$\begin{aligned}
\dot{s}_i &= -ls_i - l^2\bar{z}_i - l\bar{z}_{i+1},\ i=1,2,3,5,6\\
\dot{s}_4 &= -ls_4 - l^2\bar{z}_4 - l\left(\mathcal{L}_{\boldsymbol{f}}^4 h + \mathcal{L}_{\boldsymbol{g}}\mathcal{L}_{\boldsymbol{f}}^3 h\bar{\boldsymbol{u}}\right)\\
\dot{s}_7 &= -ls_7 - l^2\bar{z}_7 - l\left(\mathcal{L}_{\boldsymbol{f}}^3 V + \mathcal{L}_{\boldsymbol{g}}\mathcal{L}_{\boldsymbol{f}}^2 V\bar{\boldsymbol{u}}\right)\\
\hat{\epsilon}_j &= s_j + l\bar{z}_j,\ j=1,2,\cdots,7
\end{aligned} \tag{12}$$

where $l>0$ is the observer gain and $\hat{\epsilon}_j$ is the estimate of ϵ_j. By the estimates, the NDI-based virtual tracking controllers can be defined and designed as follows [3]:

$$\boldsymbol{v}_n \triangleq [v_{hn},\ v_{Vn}]^T = \boldsymbol{B}(\bar{\boldsymbol{x}})\bar{\boldsymbol{u}} \tag{13}$$

$$\begin{aligned}
v_{hn} = \boldsymbol{k}_h &\left[h_r - \bar{z}_1,\ h_r^{(1)} - \bar{z}_2 - \hat{\epsilon}_1,\ h_r^{(2)} - \bar{z}_3 - \hat{\epsilon}_2,\ h_r^{(3)} - \bar{z}_4 - \hat{\epsilon}_3\right]^T\\
&+ h_r^{(4)} - \mathcal{L}_{\boldsymbol{f}}^4 h - \hat{\epsilon}_4
\end{aligned} \tag{14}$$

$$v_{Vn} = \boldsymbol{k}_V\left[V_r - \bar{z}_5,\ V_r^{(1)} - \bar{z}_6 - \hat{\epsilon}_5,\ V_r^{(2)} - \bar{z}_7 - \hat{\epsilon}_6\right]^T + V_r^{(3)} - \mathcal{L}_{\boldsymbol{f}}^3 V - \hat{\epsilon}_7 \tag{15}$$

where $\boldsymbol{k}_h$ and $\boldsymbol{k}_V$ are the control gains of the altitude and velocity subsystems, respectively; h_r and V_r are the references of the altitude and velocity, respectively. The proposed tracking controllers (14) and (15) are constructed using the control-oriented model (6) with appropriate compensations for the model errors.

For an intuitive understanding of the design idea of the proposed controllers, we only establish the stability property under a common assumption [26, 38] that the model errors vary slowly concerning the observer dynamics (i.e., $\dot{\epsilon}_i = 0,\ i=1,2,\cdots,7$), which is reasonable if the observer

[3] To distinguish the virtual controllers here from the modified ones by the constrained allocation, a subscript 'n' is imposed on (13), (14) and (15) to emphasize that they are only normal controllers without considering any actuator constraints.

gain l is relatively large. Define the tracking errors and estimation errors as

$$\begin{aligned}
\boldsymbol{e}_h &\triangleq \left[h - h_r,\ \mathcal{L}_{\bar{\boldsymbol{F}}} h - h_r^{(1)},\ \mathcal{L}^2_{\bar{\boldsymbol{F}}} h - h_r^{(2)},\ \mathcal{L}^3_{\bar{\boldsymbol{F}}} h - h_r^{(3)}\right]^T \\
\boldsymbol{e}_V &\triangleq \left[V - V_r,\ \mathcal{L}_{\bar{\boldsymbol{F}}} V - V_r^{(1)},\ \mathcal{L}^2_{\bar{\boldsymbol{F}}} V - V_r^{(2)}\right]^T \\
\boldsymbol{e}_\epsilon &\triangleq \left[\epsilon_1 - \hat{\epsilon}_1,\ \cdots,\ \epsilon_7 - \hat{\epsilon}_7\right]^T.
\end{aligned}$$

Omitting tedious derivation yields the following error system:

$$\begin{bmatrix} \dot{\boldsymbol{e}}_h \\ \dot{\boldsymbol{e}}_V \\ \dot{\boldsymbol{e}}_\epsilon \end{bmatrix} = \begin{bmatrix} \boldsymbol{A}_{kh} & \boldsymbol{0}_{4\times 3} & \boldsymbol{\Lambda}_1 \\ \boldsymbol{0}_{3\times 4} & \boldsymbol{A}_{kV} & \boldsymbol{\Lambda}_2 \\ \boldsymbol{0}_{7\times 4} & \boldsymbol{0}_{7\times 3} & -l\boldsymbol{I}_{7\times 7} \end{bmatrix} \begin{bmatrix} \boldsymbol{e}_h \\ \boldsymbol{e}_V \\ \boldsymbol{e}_\epsilon \end{bmatrix} \tag{16}$$

where

$$\boldsymbol{A}_{kh} \triangleq \boldsymbol{A}_h - \boldsymbol{B}_h \boldsymbol{k}_h,\ \boldsymbol{A}_h \triangleq \begin{bmatrix} \boldsymbol{0}_{3\times 1} & \boldsymbol{I}_{3\times 3} \\ 0 & \boldsymbol{0}_{1\times 3} \end{bmatrix},\ \boldsymbol{B}_h \triangleq \begin{bmatrix} \boldsymbol{0}_{3\times 1} \\ 1 \end{bmatrix}$$

$$\boldsymbol{A}_{kV} \triangleq \boldsymbol{A}_V - \boldsymbol{B}_V \boldsymbol{k}_V,\ \boldsymbol{A}_V \triangleq \begin{bmatrix} \boldsymbol{0}_{2\times 1} & \boldsymbol{I}_{2\times 2} \\ 0 & \boldsymbol{0}_{1\times 2} \end{bmatrix},\ \boldsymbol{B}_V \triangleq \begin{bmatrix} \boldsymbol{0}_{2\times 1} \\ 1 \end{bmatrix}$$

and $\boldsymbol{\Lambda}_i$ $(i = 1, 2)$ are nonzero matrixes. Noting that $(\boldsymbol{A}_h, \boldsymbol{B}_h)$ and $(\boldsymbol{A}_V, \boldsymbol{B}_V)$ are both controllable, $\boldsymbol{A}_{kh}$ and $\boldsymbol{A}_{kV}$ could be Hurwitz by well tuning $\boldsymbol{k}_h$ and $\boldsymbol{k}_V$, which will eventually make the closed-loop system asymptotically stable.

Remark 1. *To pursuit the modular design, the high-level control is designed without detailed knowledge on actuators and actuator safety is handled within the low-level allocation design [12]. This implies that the infeasible virtual control commands may exist and would affect the stability of the whole control system. Actually, if we break the modular design objective, several advanced control methods considering actuator constraints are able to deal with this theoretical issue, e.g., the barrier Lyapunov function (BLF) based control [39, 40] and MPC [20, 41, 42]. The BLF method exploits the property that a barrier function grows to infinity whenever its arguments approaches some limits. By keeping the BLF bounded in the closed-loop system, it is thus guaranteed that its arguments are within the given constraints. As for the MPC, there are massive variants for*

the over-actuator systems. One of the classic paradigm is [20], where the whole control design can be divided into target calculation and model predictive tracking. In the target calculation phase, the desired states and inputs are calculated by solving a QP with mixed constraints; if it is infeasible, it is convenient to relax some constraints by introducing slack variables. Different from this classic paradigm, there are some interesting results considering the effect of the references. For example, in [42], the feasible region of desired virtual instructions is determined by characterizing the polyhedral feasible region of the pseudoinverse solution. In [41], the desired states and inputs are parameterized first, and are regarded as new decision variables in the optimization.

4. Allocation Design

The allocation task in the low level is to distribute the designed two virtual control signals, v_{hn} and v_{Vn}, into the three physical actuator inputs, δ_T, δ_E, and δ_F, within their constraints:

$$\delta_T \in [\delta_{T,\min}, \delta_{T,\max}],\ \delta_E \in [\delta_{E,\min}, \delta_{E,\max}],\ \delta_F \in [\delta_{F,\min}, \delta_{F,\max}] \tag{17}$$

where $0 < \delta_{T,\min} < \delta_{T,\max} \leq 1$, $-\pi/3 \leq \delta_{E,\min}, \delta_{F,\min} < 0$ and $0 < \delta_{E,\max}, \delta_{F,\max} \leq \pi/3$. Without loss of generality, we assume that the constraints on elevator and flap are symmetrical, i.e., $\delta_{E,\min} = -\delta_{E,\max}$ and $\delta_{F,\min} = -\delta_{F,\max}$. It is worth noting that after the dynamic extension, δ_T is not in the control input $\bar{\boldsymbol{u}}$ anymore, but the part of state $\bar{\boldsymbol{x}}$. This fact means that the conventional constrained allocation method without considering actuator dynamics would lose its effectiveness thus may compromise the safety. Here, by introducing the barrier function from [32], a dual-layer QP-based control allocator is proposed to relieve the conflict between tracking objectives and actuator constraints. Its schematic diagram is first given by Fig. 5. The outer-layer QP is used to deal with the constraints of throttle control, whose dynamics are artificially introduced by the dynamic extension approach, whereas the constraints of the remaining actuators are solved in the inner-layer.

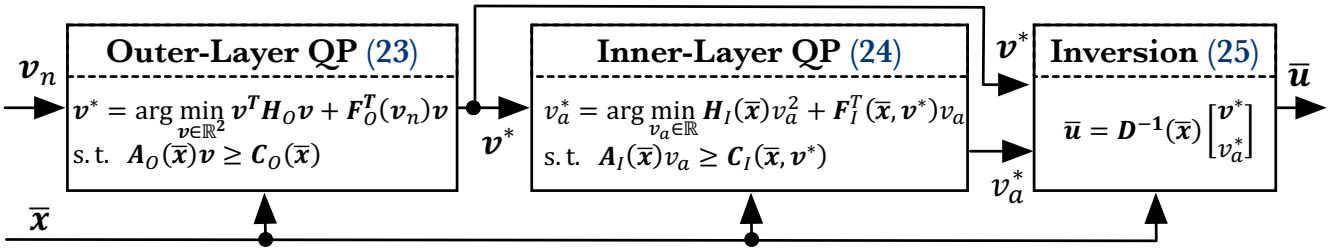

Figure 5: Schematic diagram of the proposed constrained allocator in the low level.

4.1. Allocation in the Outer Layer, Throttle

Noting the aircraft dynamics here is nonlinear, full exploration on the control gain matrix $\boldsymbol{B}(\bar{\boldsymbol{x}})$ is necessary for the constrained allocation design. To be more specific, without any additional assumptions, we only use Propositions 1 and 2 of the control-oriented model to design the constrained allocator. Since we have already stated in Lemma 1 that $\text{rank}(\boldsymbol{B}(\bar{\boldsymbol{x}})) = 2$ holds for the considered aircraft working on its normal condition, it is always possible to find a vector $\boldsymbol{P}(\bar{\boldsymbol{x}}) \in \mathbb{R}^{1\times 3}$ such that

$$\text{rank}\left(\begin{bmatrix}\boldsymbol{B}(\bar{\boldsymbol{x}}) \\ \boldsymbol{P}(\bar{\boldsymbol{x}})\end{bmatrix}\right) = 3.$$

By reviewing Proposition 2, $b_{11}(\bar{\boldsymbol{x}})b_{22}(\bar{\boldsymbol{x}}) - b_{12}(\bar{\boldsymbol{x}})b_{21}(\bar{\boldsymbol{x}}) \neq 0$, if $\boldsymbol{P}(\bar{\boldsymbol{x}})$ is chosen to be $\begin{bmatrix}0 & 0 & 1\end{bmatrix}$, the above-mentioned full rank requirement is satisfied naturally. Moreover, if the allocator is defined as $v_a \triangleq \boldsymbol{P}(\bar{\boldsymbol{x}})\bar{\boldsymbol{u}}$, the flap surface would act as the allocator, and the constraints on the flap can be simply transferred into those on the allocator. This relation can be explicitly written as follows:

$$\begin{bmatrix}\boldsymbol{v}_n \\ v_a\end{bmatrix} = \begin{bmatrix}\boldsymbol{B}(\bar{\boldsymbol{x}}) \\ \boldsymbol{P}(\bar{\boldsymbol{x}})\end{bmatrix}\bar{\boldsymbol{u}} = \begin{bmatrix}b_{11}(\bar{\boldsymbol{x}}) & b_{12}(\bar{\boldsymbol{x}}) & b_{13}(\bar{\boldsymbol{x}}) \\ b_{21}(\bar{\boldsymbol{x}}) & b_{22}(\bar{\boldsymbol{x}}) & b_{23}(\bar{\boldsymbol{x}}) \\ 0 & 0 & 1\end{bmatrix}\bar{\boldsymbol{u}} \triangleq \boldsymbol{D}(\bar{\boldsymbol{x}})\bar{\boldsymbol{u}}. \tag{18}$$

The invertibility of $\boldsymbol{D}(\bar{\boldsymbol{x}})$ can be guaranteed by $\det(\boldsymbol{D}(\bar{\boldsymbol{x}})) = b_{11}(\bar{\boldsymbol{x}})b_{22}(\bar{\boldsymbol{x}}) - b_{12}(\bar{\boldsymbol{x}})b_{21}(\bar{\boldsymbol{x}}) \neq 0$. We then can denote its inverse as $\boldsymbol{D}^{-1}(\bar{\boldsymbol{x}}) = [d_{ij}(\bar{\boldsymbol{x}})]_{3\times 3}$, whose elements can be explicitly given by using the adjugate of $\boldsymbol{D}(\bar{\boldsymbol{x}})$. Noting that $\text{adj}(\boldsymbol{D}(\bar{\boldsymbol{x}}))(1,3) = b_{12}(\bar{\boldsymbol{x}})b_{23}(\bar{\boldsymbol{x}}) - b_{13}(\bar{\boldsymbol{x}})b_{22}(\bar{\boldsymbol{x}})$, keeping

Proposition 1 in mind, we will have $d_{13}(\bar{\boldsymbol{x}}) = 0$, and hence the following relation holds:

$$\begin{bmatrix} \delta_t \\ \delta_E \\ \delta_F \end{bmatrix} = \begin{bmatrix} d_{11}(\bar{\boldsymbol{x}}) & d_{12}(\bar{\boldsymbol{x}}) & 0 \\ d_{21}(\bar{\boldsymbol{x}}) & d_{22}(\bar{\boldsymbol{x}}) & d_{23}(\bar{\boldsymbol{x}}) \\ 0 & 0 & 1 \end{bmatrix} \begin{bmatrix} v_{hn} \\ v_{Vn} \\ v_a \end{bmatrix}. \tag{19}$$

From (19), we can tell that the input to the throttle dynamics, δ_t, is only affected by the high-level tracking controllers, v_{hn} and v_{Vn}, which implies that the previous high-level controllers should be modified to meet the requirement of throttle constraints. The modified ones can be denoted as v_h and v_V, $\boldsymbol{v} \triangleq [v_h,\ v_V]^T$. It is worth highlighting that (18) and (19) still hold for the modified virtual controllers as the relation between the virtual inputs and control inputs only depends on the control-oriented model and would not be changed when the high-level controllers are changed.

Next, we will first introduce the following lemma, which is significant in handling the throttle constraints. Its proof can be directly deducted from the comparison lemma.

Lemma 2. *For a scaled function $f(t)$, suppose that $f(0) \geq 0$ and there exists a constant $r \geq 0$ such that $f^{(1)}(t) \geq -rf(t)$ holds for $t \geq 0$, then $f(t) \geq 0$ holds for $t \geq 0$.*

In what follows, detailed steps are given to recursively solve the constrained allocation problem using Lemma 2.

a) *Step One:* Define $f_1(t) \triangleq (\delta_{T,\max} - \delta_T)(\delta_T - \delta_{T,\min})$. The objective of the constrained allocation here is to guarantee that $f_1(t) \geq 0$. It is reasonable to tune the initial throttle within the constraints, i.e., $\delta_T(0) \in [\delta_{T,\min}, \delta_{T,\max}] \Leftrightarrow f_1(0) \geq 0$. By continuing the derivation of $f_1(t)$, $f_1^{(1)}(t) = -2\dot{\delta}_T\delta_T + (\delta_{T,\min} + \delta_{T,\max})\dot{\delta}_T$, we have that $f_1^{(1)}(t)$ is not directly controllable due to the deficiency of δ_t.

b) *Step Two:* Define $f_2(t) \triangleq rf_1(t) + f_1^{(1)}(t),\ r \geq 0$. The objective of this step is to guarantee that $f_2(t) \geq 0$, which will lead $f_1(t) \geq 0$ by Lemma 2 and $f_1(0) \geq 0$ from Step One. Noting that $\dot{\delta}_T(0)$ is also tunable due to the artificial actuator dynamics, it is easy to guarantee

$f_2(0) \geq 0$, that is:

$$\begin{aligned}
&\dot{\delta}_T(0)\left(\delta_{T,\min}+\delta_{T,\max}-2\delta_T(0)\right)+r\left(\delta_T(0)-\delta_{T,\min}\right)\left(\delta_{T,\max}-\delta_T(0)\right)\geq 0\\
\Leftrightarrow&\begin{cases}
\dot{\delta}_T(0)\geq -\dfrac{r\left(\delta_T(0)-\delta_{T,\min}\right)\left(\delta_{T,\max}-\delta_T(0)\right)}{\delta_{T,\min}+\delta_{T,\max}-2\delta_T(0)}, & \\
\qquad\qquad\qquad\qquad \text{if } \delta_T(0)\in\left(\dfrac{\delta_{T,\min}+\delta_{T,\max}}{2},\delta_{T,\max}\right] & \\
\dot{\delta}_T(0)\in\mathbb{R}, \qquad\qquad \text{if } \delta_T(0)=\dfrac{\delta_{T,\min}+\delta_{T,\max}}{2} & \\
\dot{\delta}_T(0)\leq -\dfrac{r\left(\delta_T(0)-\delta_{T,\min}\right)\left(\delta_{T,\max}-\delta_T(0)\right)}{\delta_{T,\min}+\delta_{T,\max}-2\delta_T(0)}, & \\
\qquad\qquad\qquad\qquad \text{if } \delta_T(0)\in\left[\delta_{T,\min},\dfrac{\delta_{T,\min}+\delta_{T,\max}}{2}\right). &
\end{cases}
\end{aligned} \tag{20}$$

We can tell that inequality (20) is always feasible for $\dot{\delta}_T(0)$, if $\delta_T(0)\in[\delta_{T,\min},\delta_{T,\max}]$. Next, in order to guarantee $f_2(t)\geq 0$, only $f_2^{(1)}(t)\geq -rf_2(t)$ is required, which is equivalent to the following compact form:

$$\boldsymbol{A}_{O_1}(\bar{\boldsymbol{x}})\boldsymbol{v}\geq \boldsymbol{C}_{O_1}(\bar{\boldsymbol{x}}) \tag{21}$$

where

$$\begin{aligned}
\boldsymbol{A}_{O_1}(\bar{\boldsymbol{x}})&\triangleq\left(\delta_{T,\min}+\delta_{T,\max}-2\delta_T\right)\begin{bmatrix}d_{11}(\bar{\boldsymbol{x}}) & d_{12}(\bar{\boldsymbol{x}})\end{bmatrix}\\
\boldsymbol{C}_{O_1}(\bar{\boldsymbol{x}})&\triangleq -r^2(\delta_{T,\max}-\delta_T)(\delta_T-\delta_{T,\min})-2r\dot{\delta}_T(\delta_{T,\min}+\delta_{T,\max}-2\delta_T)+2\dot{\delta}_T^2.
\end{aligned}$$

Apart from the throttle, the elevator and flap should also be considered in the outer layer. From the expression in (19), $d_{21}(\bar{\boldsymbol{x}})v_h+d_{22}(\bar{\boldsymbol{x}})v_V=\delta_E-d_{23}(\bar{\boldsymbol{x}})\delta_F$, if the virtual tracking controllers are extremely chosen, the inner-layer allocation will be impossible to implement. For the feasibility of the inner layer, v_h and v_V are required to satisfy:

$$d_{21}(\bar{\boldsymbol{x}})v_h+d_{22}(\bar{\boldsymbol{x}})v_V\in\left[-\delta_{E,\max}-|d_{23}(\bar{\boldsymbol{x}})|\delta_{F,\max},\delta_{E,\max}+|d_{23}(\bar{\boldsymbol{x}})|\delta_{F,\max}\right],$$

which can also be compactly expressed as:

$$\boldsymbol{A}_{O_2}(\bar{\boldsymbol{x}})\boldsymbol{v}\geq \boldsymbol{C}_{O_2}(\bar{\boldsymbol{x}}) \tag{22}$$

where

$$\boldsymbol{A}_{O_2}(\bar{\boldsymbol{x}}) \triangleq \begin{bmatrix} d_{21}(\bar{\boldsymbol{x}}) & d_{22}(\bar{\boldsymbol{x}}) \\ -d_{21}(\bar{\boldsymbol{x}}) & -d_{22}(\bar{\boldsymbol{x}}) \end{bmatrix}, \ \boldsymbol{C}_{O_2}(\bar{\boldsymbol{x}}) \triangleq \begin{bmatrix} -\delta_{E,\max} - |d_{23}(\bar{\boldsymbol{x}})|\delta_{F,\max} \\ -\delta_{E,\max} - |d_{23}(\bar{\boldsymbol{x}})|\delta_{F,\max} \end{bmatrix}.$$

Combining (21) and (22) together, and noting the nominal controllers in (14) and (15), the high-level tracking design can be modified by a standard QP problem, as follows:

$$\begin{aligned} \boldsymbol{v}^* &= \arg \min_{v_h \in \mathbb{R},\ v_V \in \mathbb{R}} \varrho_h (v_h - v_{hn})^2 + \varrho_V (v_V - v_{Vn})^2 \\ &= \arg \min_{\boldsymbol{v} \in \mathbb{R}^2} \ \boldsymbol{v}^T \boldsymbol{H}_O \boldsymbol{v} + \boldsymbol{F}_O^T(\boldsymbol{v}_n) \boldsymbol{v} \\ &\text{s.t. } \boldsymbol{A}_O(\bar{\boldsymbol{x}}) \boldsymbol{v} \geq \boldsymbol{C}_O(\bar{\boldsymbol{x}}) \end{aligned} \tag{23}$$

where

$$\boldsymbol{H}_O \triangleq \begin{bmatrix} \varrho_h & 0 \\ 0 & \varrho_V \end{bmatrix}, \ \boldsymbol{F}_O(\boldsymbol{v}_n) \triangleq \begin{bmatrix} -2\varrho_h v_{hn} \\ -2\varrho_V v_{Vn} \end{bmatrix}$$

$$\boldsymbol{A}_O(\bar{\boldsymbol{x}}) \triangleq \begin{bmatrix} \boldsymbol{A}_{O_1}(\bar{\boldsymbol{x}}) \\ \boldsymbol{A}_{O_2}(\bar{\boldsymbol{x}}) \end{bmatrix}, \ \boldsymbol{C}_O(\bar{\boldsymbol{x}}) \triangleq \begin{bmatrix} \boldsymbol{C}_{O_1}(\bar{\boldsymbol{x}}) \\ \boldsymbol{C}_{O_2}(\bar{\boldsymbol{x}}) \end{bmatrix}$$

and $\varrho_h > 0$ and $\varrho_V > 0$ are the weights to prioritize different virtual control inputs.

Remark 2. *To guarantee the safety of the throttle, the constraints not only on $\delta_T(0)$, but also on $\dot{\delta}_T(0)$ are necessary, where the constraint on $\dot{\delta}_T(0)$ is given to avoid several extreme cases. For example, if $\delta_T(0) = \delta_{T,\min}$ and $\dot{\delta}_T(0) < 0$, due to the continuity of the throttle model, there must exist a time instance $t_1 > 0$ such that $\delta_T(t_1) < \delta_{T,\min}$, which inevitably breaks the safety requirement. A similar case would happen if $\delta_T(0) = \delta_{T,\max}$ and $\dot{\delta}_T(0) > 0$.*

Remark 3. *By the structure of the cost function in (23), the virtual tracking controllers, v_h and v_V, are only modified when the constraints in (21) and (22) are active. Once active, the conflict between tracking objectives and actuator constraints will appear, and the solution of (23) is given in a higher priority of safety. This phenomenon can be well demonstrated by Fig. 7 in the subsequent simulation.*

4.2. Allocation in the Inner Layer, Elevator and Flap

With the assist of the outer-layer allocation, the inner-layer task would be simple and can also be formulated as a QP problem for the consistency of the theoretical formulation, as follows:

$$\begin{aligned} v_a^* &= \arg\min_{v_a\in\mathbb{R}} \ \varrho_E\left(\delta_E-\delta_{Edes}\right)^2+\varrho_F\left(\delta_F-\delta_{Fdes}\right)^2 \\ &= \arg\min_{v_a\in\mathbb{R}} \ \boldsymbol{H}_I(\bar{\boldsymbol{x}})v_a^2+\boldsymbol{F}_I(\bar{\boldsymbol{x}},\boldsymbol{v}^*)v_a \\ &\text{s.t. } \boldsymbol{A}_I(\bar{\boldsymbol{x}})v_a\geq \boldsymbol{C}_I(\bar{\boldsymbol{x}},\boldsymbol{v}^*) \end{aligned} \tag{24}$$

where

$$\begin{aligned} \boldsymbol{H}_I(\bar{\boldsymbol{x}}) &\triangleq \varrho_E d_{23}^2(\bar{\boldsymbol{x}})+\varrho_F \\ \boldsymbol{F}_I(\bar{\boldsymbol{x}},\boldsymbol{v}^*) &\triangleq 2\varrho_E\begin{bmatrix} d_{21}(\bar{\boldsymbol{x}}) & d_{22}(\bar{\boldsymbol{x}})\end{bmatrix}\boldsymbol{v}^*-2\varrho_E\delta_{Edes}-2\varrho_F\delta_{Fdes} \\ \boldsymbol{A}_I(\bar{\boldsymbol{x}}) &\triangleq \begin{bmatrix} d_{23}(\bar{\boldsymbol{x}}) \\ -d_{23}(\bar{\boldsymbol{x}}) \\ 1 \\ -1\end{bmatrix},\ \boldsymbol{C}_I(\bar{\boldsymbol{x}},\boldsymbol{v}^*)\triangleq \begin{bmatrix} -\delta_{E,\max}-\begin{bmatrix} d_{21}(\bar{\boldsymbol{x}}) & d_{22}(\bar{\boldsymbol{x}})\end{bmatrix}\boldsymbol{v}^* \\ -\delta_{E,\max}+\begin{bmatrix} d_{21}(\bar{\boldsymbol{x}}) & d_{22}(\bar{\boldsymbol{x}})\end{bmatrix}\boldsymbol{v}^* \\ -\delta_{F,\max} \\ -\delta_{F,\max}\end{bmatrix} \end{aligned}$$

and $\boldsymbol{v}^*$ is the solution of the outer-layer QP (23); $\varrho_E>0$ and $\varrho_F>0$ are the weights to prioritize different control surfaces; δ_{Edes} and δ_{Fdes} are the desired values.

By (18), (23) and (24), the final controller could be implemented to close the control loop, as follows:

$$\bar{\boldsymbol{u}}=\boldsymbol{D}^{-1}(\bar{\boldsymbol{x}})\begin{bmatrix}\boldsymbol{v}^* \\ v_a^*\end{bmatrix}. \tag{25}$$

The following theorem is presented to conclude this section, whose proof is straightforward from the allocation design.

Theorem 1. *Consider the aircraft (10) under the controller (25). Suppose that the initial states of the actuator are well tuned such that* $\delta_T(0)\in[\delta_{T,\min},\delta_{T,\max}]$ *and* $\dot{\delta}_T(0)$ *satisfies (20); QP problems (23) and (24) are both feasible over the operating range of interest. Then, (17) holds for* $t\geq 0$.

Remark 4. *If the constraints in the outer-layer QP (23) are not active, only the inner-layer one*

(24) operates in the whole allocation process. In such a case, the proposed method will degenerate into the conventional control allocation method [12, Sec. 2.2].

Remark 5. *Although the computational effort is always the barrier when one tries to solve the constrained optimization problem online, it is not apparent in this paper due to the low dimensions. The dimensions of the decision variables in the outer-layer QP and inner-layer QP are 2 and 1, respectively, which makes the proposed allocator possible to be real-timely implemented in the small UAV system, as shown by the computation time in Fig. 12. On the other hand, algorithms on solving such a constrained optimization problem are relatively well-developed, and using different algorithms would take different computational effort, e.g., multi-parametric QP solver [43].*

Remark 6. *To guarantee the stability of the whole system, we need to consider the control Lyapunov function (CLF) as an additional constraint of the outer-layer QP [32], which however, will bring more computation cost. At first, we need to rewrite the error system (16) to make the virtual control $\boldsymbol{v}$ explicit:*

$$\begin{aligned} \dot{\boldsymbol{e}} &= \boldsymbol{A}_e \boldsymbol{e} + \boldsymbol{A}_\epsilon \boldsymbol{e}_\epsilon + \boldsymbol{B}_v \boldsymbol{v} \\ \dot{\boldsymbol{e}}_\epsilon &= -l \boldsymbol{I}_{7\times 7} \boldsymbol{e}_\epsilon \end{aligned} \tag{26}$$

where $\boldsymbol{A}_e$, $\boldsymbol{A}_\epsilon$, and $\boldsymbol{B}_v$ are system matrices. Since the tracking error $\boldsymbol{e}$ is measurable, its CLF can be set as the constraint of QP. Based on the property of the cascaded system, a sufficient condition for the stability of the error system (26) is that the subsystem $\dot{\boldsymbol{e}} = \boldsymbol{A}_e \boldsymbol{e} + \boldsymbol{B}_v \boldsymbol{v}$ is stable, that is:

$$\dot{W}(\boldsymbol{e}) \leq -cW(\boldsymbol{e}) \tag{27}$$

where $W(\boldsymbol{e}) \triangleq \boldsymbol{e}^T \boldsymbol{P} \boldsymbol{e}$ is the CLF, $\boldsymbol{P}$ is a positive definite matrix; c is a positive constant. However, the condition (27) is usually infeasible as the effect of both the estimation error system and actuator constraint is not considered. Such a constraint represented by the CLF condition has to be relaxed as follows:

$$\begin{aligned} &\dot{W}(\boldsymbol{e}) \leq -cW(\boldsymbol{e}) + d \\ \Leftrightarrow &2\boldsymbol{e}^T \boldsymbol{P} \boldsymbol{B}_v \boldsymbol{v} \leq -cW(\boldsymbol{e}) - \boldsymbol{e}^T (\boldsymbol{A}_e^T \boldsymbol{P} + \boldsymbol{P} \boldsymbol{A}_e) \boldsymbol{e} + d \end{aligned} \tag{28}$$

where d is a constant. With this condition (28), the new outer-layer QP is given by follows:

$$\begin{aligned}
\begin{bmatrix} \boldsymbol{v}^* \\ d^* \end{bmatrix} &= \arg \min_{v_h \in \mathbb{R},\ v_V \in \mathbb{R},\ d \in \mathbb{R}} \varrho_h (v_h - v_{hn})^2 + \varrho_V (v_V - v_{Vn})^2 + \varrho_d d^2 \\
&= \arg \min_{\boldsymbol{v} \in \mathbb{R}^2,\ d \in \mathbb{R}} \ \boldsymbol{v}^T \boldsymbol{H}_O \boldsymbol{v} + \boldsymbol{F}_O^T(\boldsymbol{v}_n)\boldsymbol{v} + \varrho_d d^2 \qquad (29) \\
s.t.\ & \boldsymbol{A}_O(\bar{\boldsymbol{x}})\boldsymbol{v} \geq \boldsymbol{C}_O(\bar{\boldsymbol{x}}) \\
& 2\boldsymbol{e}^T \boldsymbol{P} \boldsymbol{B}_v \boldsymbol{v} \leq -cW(\boldsymbol{e}) - \boldsymbol{e}^T(\boldsymbol{A}_e^T \boldsymbol{P} + \boldsymbol{P}\boldsymbol{A}_e)\boldsymbol{e} + d
\end{aligned}$$

where $\varrho_d \geq 0$ is the weight to prioritize d. Compared with the original outer-layer QP (23), the soft constraint (28) based on CLF is added and the relaxation parameter d is regarded as a new decision variable. If d^* is positive, the stability and safety objectives conflict and the proposed allocation would slow down the convergence rate; if $d^* = 0$, these two objectives do not conflict.

5. Simulation Results

In this section, the AeroSim aeronautical simulation is employed to verify the proposed control method, where the detailed aerodynamic coefficients are given by Table B.4. The AeroSim simulation provides a complete set of tools for the rapid development of high degree-of-freedom nonlinear aircraft dynamic models [33], and hence, is famous for the control performance test of Aerosonde aircraft [5, 8, 9, 10]. In order to simulate the real flight environment, the wind effects are included by considering both the Dryden wind turbulence model and wind gust model [44]. Dryden wind turbulence model uses the Dryden spectral representation to add turbulence to the aircraft model by passing band-limited white noise through appropriate forming filters. Wind gust model implements a wind gust of the standard 1-cosine shape. This gust model can be applied to each axis individually or to all three axes at once. In the simulation, the used Lie derivatives are offline calculated by Symbolic Math Toolbox and the dual-layer QP is online solved by Optimization

Toolbox of Matlab. Initial conditions of the simulation are set as the trims as follows:

$$h(0) = 10,\ V(0) = 10,\ \gamma(0) = 0,\ \alpha(0) = 0.3193,\ q(0) = 0.0025$$
$$\delta_T(0) = 0.5363,\ \dot{\delta}_T(0) = 0$$
$$s_1(0) = -50.04,\ s_2(0) = -11.09,\ s_3(0) = -0.8652,\ s_4(0) = 7.788$$
$$s_5(0) = -53.55,\ s_6(0) = 4.446,\ s_7(0) = -2.191,$$

and allocation/control parameters are listed as follows:

$$\delta_{Edes} = 0,\ \delta_{Fdes} = 0,\ \varrho_h = \varrho_V = \varrho_E = \varrho_F = 1,\ r = 100$$
$$\delta_{T,\min} \in \{0.3, 0.4\},\ \delta_{T,\max} \in \{0.65, 0.7\},\ \delta_{E,\max}, \delta_{F,\max} \in \{\pi/3, 5\pi/18, 2\pi/9\}$$
$$\boldsymbol{k}_h = \begin{bmatrix} \omega_h^4 & 4\omega_h^3 & 6\omega_h^2 & 4\omega_h \end{bmatrix},\ \omega_h = 3$$
$$\boldsymbol{k}_V = \begin{bmatrix} \omega_V^3 & 3\omega_V^2 & 3\omega_V \end{bmatrix},\ \omega_V = 3,\ l = 15.$$

Here, the bandwidths of the altitude and velocity subsystems are tuned to be the same, i.e., $\omega_h = \omega_V$. The following tests are mainly focused on three aspects: Case I is given to show the advantages of the proposed control allocation method against two representative methods, i.e., MPC and pseudoinverse; Case II is given to show the validity of the proposed control allocation method under different actuator constraints; Case III is given to show the improvement of tracking precision of the proposed control method against a classical control method, i.e., NDI.

5.1. Case I. The proposed control allocation vs. MPC-based control allocation vs. pseudoinverse-based control allocation

In this case study, MPC-based control allocation [21] and pseudoinverse-based control allocation [12, Sec. 2.1] are implemented for comparison. The actuator constraints are set the same, i.e., $[30\%, 70\%]$ of throttle and $[-60^\circ, 60^\circ]$ of both elevator and flap; and the high-level controllers of these three allocation methods are the same, i.e., (13), (14) and (15). Before directly applying the MPC-based control allocation, calculating $\boldsymbol{B}(\bar{\boldsymbol{x}})$ in (8) at the trim and discretizing the actuator dynamics are needed to be pre-completed. In contrast, the pseudoinverse-based control allocation

is quite straightforward to be applied just based on the relation between the virtual and physical controllers, i.e., (13). The aircraft and actuator states under the different allocation methods are illustrated in Fig. 6, respectively, and their indexes of the tracking errors in the whole period, i.e., from 0 to 40 sec, are given by Table 1. From the simulation results, the tracking objectives are achieved by the proposed and pseudoinverse-based control allocation methods, while large offset errors exist in the MPC-based control allocation method once the references have been changed. The main reason is that only one trim of the control gain matrix $\boldsymbol{B}(\bar{\boldsymbol{x}})$ cannot cover the whole range of operation; although the gain schedule strategy can relieve this problem by calculating multiple trims, more efforts on calculation and tuning are necessary in advance. As for the actuator safety, it can be guaranteed by the proposed and the MPC-based control allocation methods. However, the elevator and flap under the MPC-based control allocation method severely oscillates when the altitude reference increases. The throttle under the pseudoinverse-based control allocation method is out of the given constraints when the altitude reference increases, which breaks the safety requirement here.

Besides, the virtual control inputs $\boldsymbol{v}_n$ and the optimized ones $\boldsymbol{v}^*$ of the considered three control allocation methods are all given by Figs. 7 to 9. In Fig. 9, the curves of $\boldsymbol{v}_n$ and $\boldsymbol{v}^*$ totally overlap, which implies that the pseudoinverse-based control allocation is not able to deal with the actuator constraints. In contrast, as shown in Fig. 7, these two curves under the proposed control allocation method also overlap during the most time, but branch when the references change, which is corresponding to the activation of throttle constraint. In Fig. 8, large offset errors exist between $\boldsymbol{v}_n$ and $\boldsymbol{v}^*$ when the references change, leading to the tracking errors in Fig. 6.

Table 1: Performance indexes of Case I

Methods	Altitude tracking errors $\int_{t_0}^{t_1}(h_r-h)^2dt$	Velocity tracking errors $\int_{t_0}^{t_1}(V_r-V)^2dt$
The proposed control allocation	13.5807	87.9289
The MPC-based control allocation	18.6943	1318.2705
The pseudoinverse-based control allocation	12.0145	47.9677

5.2. Case II. The proposed control allocation under different constraints

To better study the allocation performance in the outer and inner layers, the constraints of both layers are artificially changed, as explicitly shown in the legends of Figs. 10 and 11. The

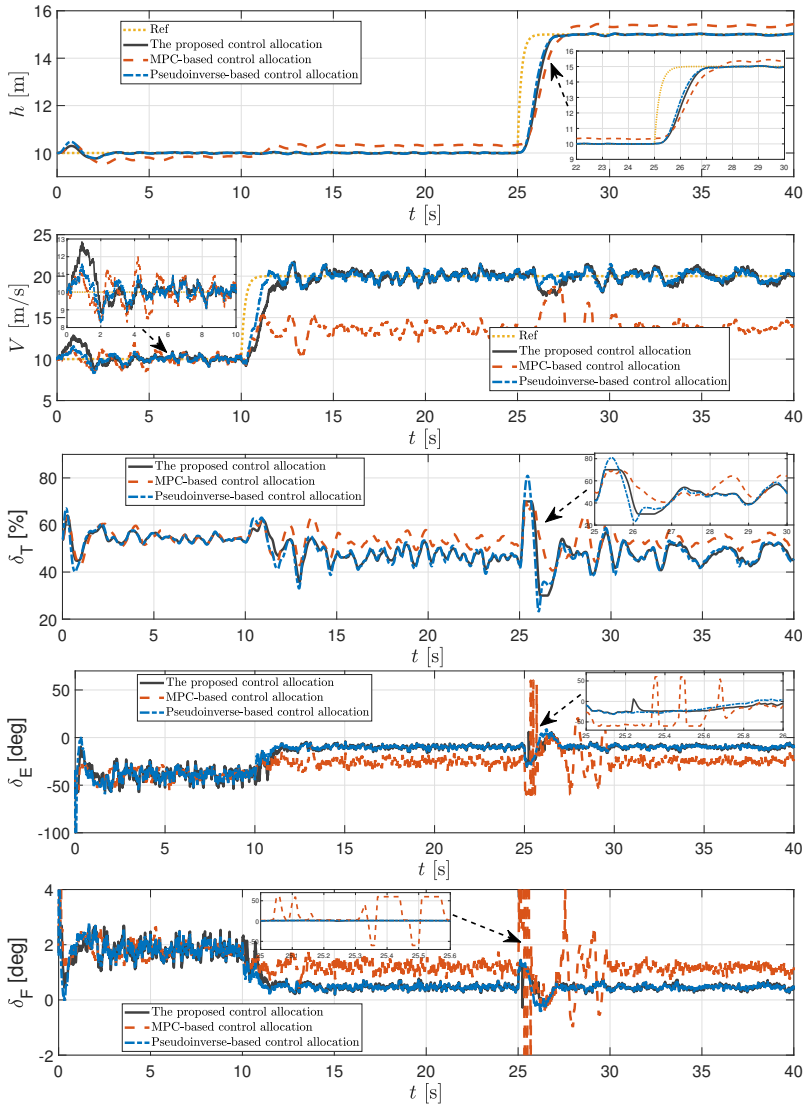

Figure 6: Allocation test results under different allocation methods.

tracking error indexes under different constraints are given by Table 2. It is worth noting that the tracking objectives are achieved in the steady state and all the actuator states are within the given constraints. It can also be observed by the simulation results that the tracking performance of the altitude and velocity are affected by constraints in both the outer and inner layers. This phenomenon can be explained by (21) and (22), which are the constraints to keep the throttle safe and inner-layer optimization feasible. These two constraints will directly affect the optimized virtual control input $\boldsymbol{v}^*$ via (23), which will finally affect the tracking dynamics.

To determine the real time capability of the proposed allocation, its calculation time under the constraints $\delta_T \in [30\%, 70\%]$, $\delta_{E,F} \in [-60°, 60°]$ is given by Fig. 12. The calculation time of

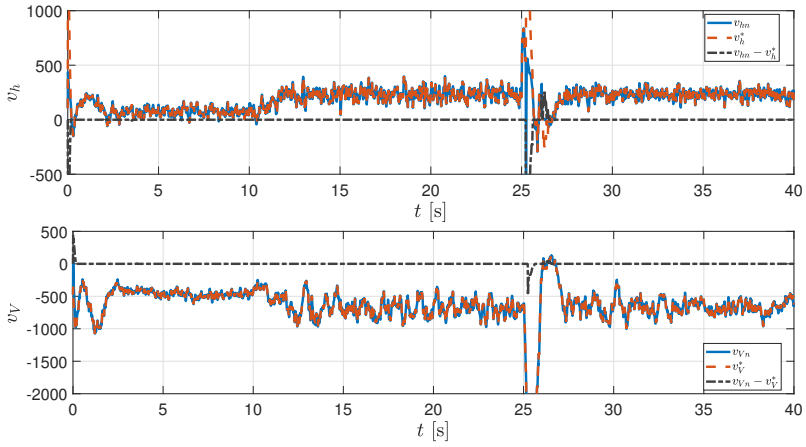

Figure 7: Virtual control inputs of the proposed control allocation.

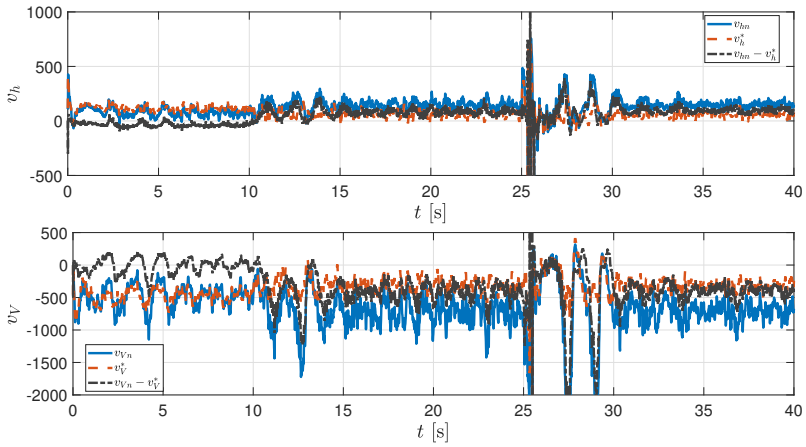

Figure 8: Virtual control inputs of the MPC-based control allocation.

each layer is less than 15% of the sample time (0.01s) even at the maximum and is around 5% on the average, which implies that the real time capability can be guaranteed. This is because the dimensions of the decision variables in both layers are low, i.e, 2 decision variables in the outer layer and 1 decision variable in the inner layer.

5.3. Case III. The proposed controller vs. NDI-based controller

In this test, we only focus on the tracking performance of different control methods, but with the same control allocation. The constraints are set as $[30\%, 70\%]$ of throttle and $[-60°, 60°]$ of both elevator and flap. The proposed controllers, (13), (14) and (15), and the conventional NDI-based controllers are studied here to show the improvement of DOs on the tracking performance. The comparisons on the tracking performance are shown by Fig. 13 and the performance indexes

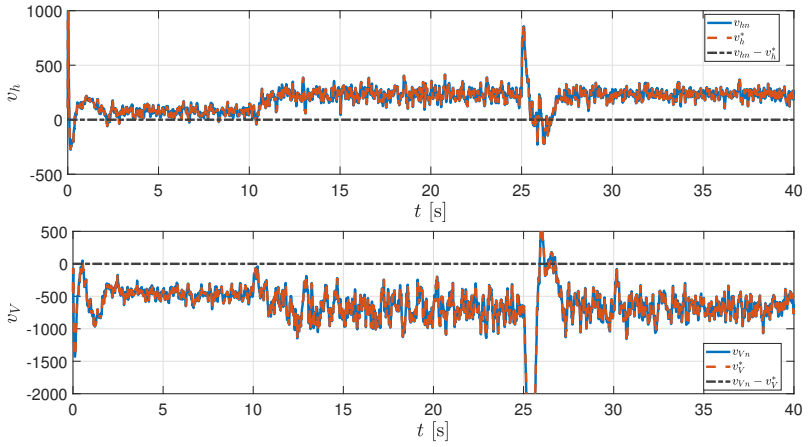

Figure 9: Virtual control inputs of the pseudoinverse-based control allocation.

Table 2: Performance indexes of Case II

Constraints	Altitude tracking errors $\int_{t_0}^{t_1}(h_r - h)^2 dt$	Velocity tracking errors $\int_{t_0}^{t_1}(V_r - V)^2 dt$
$\delta_T \in [30\%, 70\%],\ \delta_{E,F} \in [-60°, 60°]$	983.0947	656.2319
$\delta_T \in [40\%, 70\%],\ \delta_{E,F} \in [-60°, 60°]$	982.4627	639.8967
$\delta_T \in [40\%, 65\%],\ \delta_{E,F} \in [-60°, 60°]$	1045.2535	715.5899
$\delta_T \in [30\%, 70\%],\ \delta_{E,F} \in [-50°, 50°]$	983.0518	656.8268
$\delta_T \in [30\%, 70\%],\ \delta_{E,F} \in [-40°, 40°]$	986.9767	643.1389

are given by Table 3. From the performance indexes in Table 3, it can be concluded that the proposed controller has improved the tracking precisions of the altitude and velocity by 24.27% and 17.37%, respectively.

Table 3: Performance indexes of Case III

Methods	Altitude tracking errors $\int_{t_0}^{t_1}(h_r - h)^2 dt$	Velocity tracking errors $\int_{t_0}^{t_1}(V_r - V)^2 dt$
The proposed controller	983.0947	656.2319
The NDI-based controller	1298.1911	794.2346

6. Conclusion

Flight control design for nonlinear over-actuated aircraft faces several challenges, such as the nonlinear nature of the aircraft behavior due to the complex motion and aerodynamics and multiple actuators with physical constraints. To this end, the longitudinal flight control of the Aerosonde aircraft has been studied in this paper. A control-oriented model with well-defined relative degrees has been firstly established by only simplifying several parts of aerodynamics, whose applicability can be proved to sufficiently cover the normal operating range of the aircraft. The model

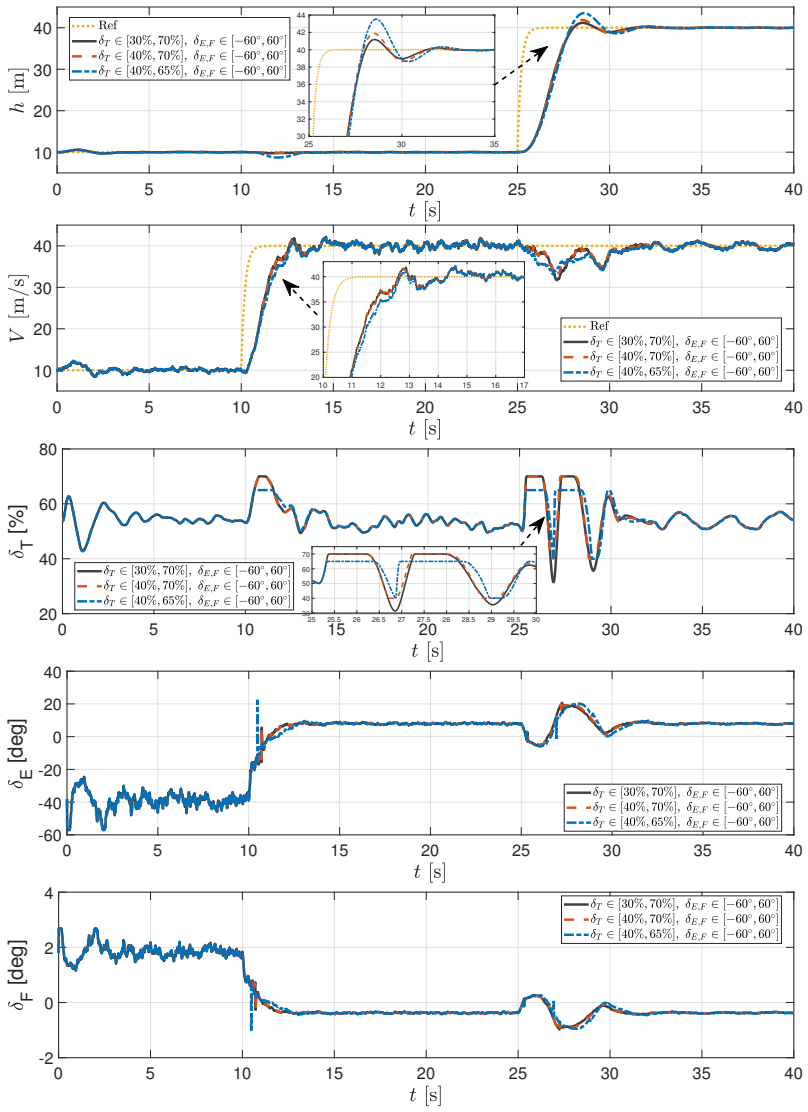

Figure 10: Allocation tests under different constraints of the throttle.

errors have been estimated by the disturbance observers and compensated in the nonlinear dynamic inversion-based controllers towards high-precision tracking. It is interesting to find that the throttle signal is only affected by the control commands from the high level, which is quite different from the conventional allocation framework. Consequently, we have proposed a new dual-layer quadratic programming (QP)-based control allocation, which can relieve the conflict between tracking objectives and actuator constraints. The outer-layer QP focuses on the constraints of throttle, whose dynamics is artificially generated by the high-level design, along with the feasibility of the inner-layer QP, whilst the constraints of the remaining actuators, i.e., the elevator and flap, have been solved in the inner-layer design. High fidelity simulations have been

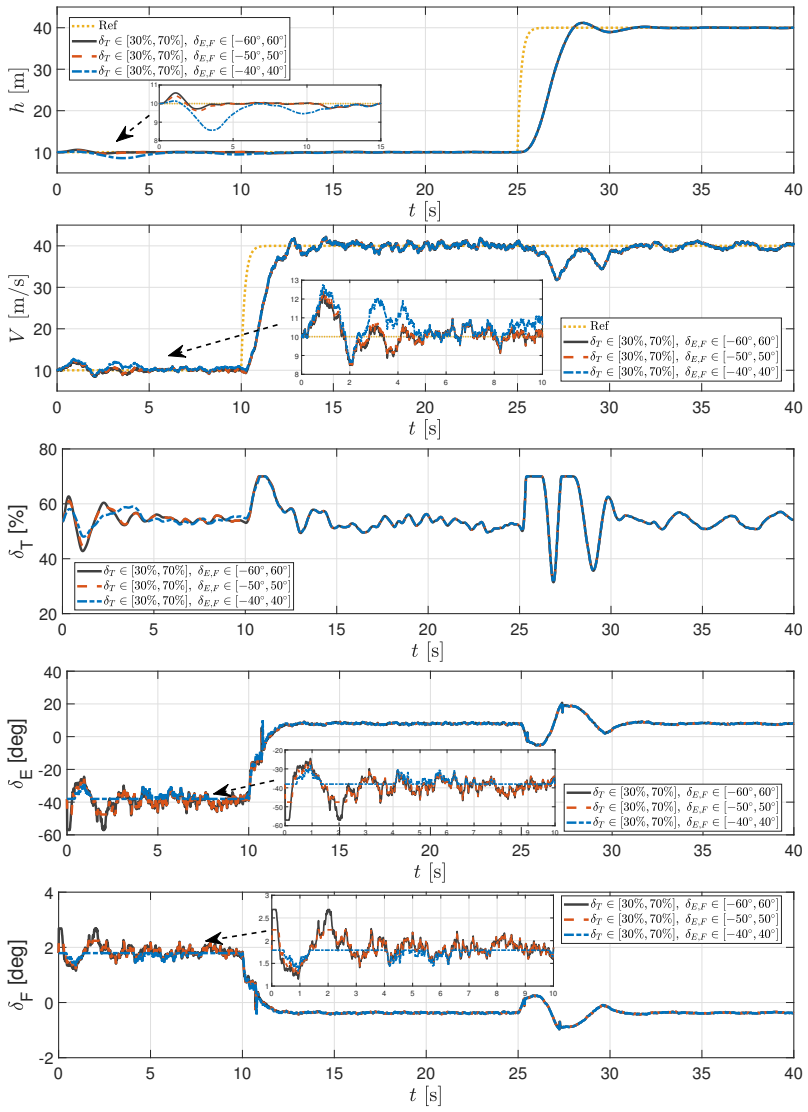

Figure 11: Allocation tests under different constraints of the elevator and flap.

implemented to demonstrate the effectiveness of the proposed method in trajectory tracking and constrained allocation. Although only the longitudinal dynamics of the Aerosonde is studied here, it is envisaged that the proposed method can be extended to control more general nonlinear over-actuated systems with physical constraints.

Acknowledgement

The authors would like to thank the thorough review and valuable suggestions from the associate editor and the anonymous reviewers. Hyondong Oh's involvement in this research was supported by Agency for Defense Development under the grant No. U19176JF.

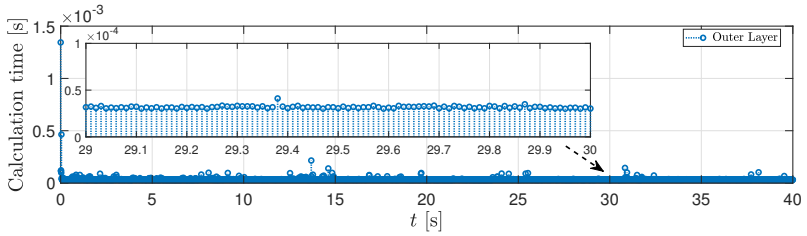

a)

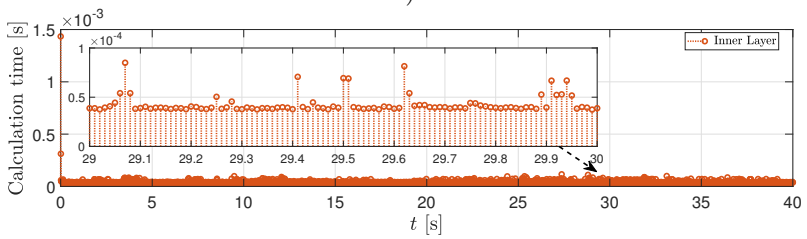

b)

Figure 12: Computation time of the proposed control allocation. a) Outer layer. b) Inner layer.

Appendix A. Control Gain Matrix

The elements of the control gain matrix $\boldsymbol{B}(\bar{\boldsymbol{x}})$ are given as follows:

$$
\begin{aligned}
b_{11}(\bar{\boldsymbol{x}}) &= \frac{C_{\text{prop}} K_{\text{motor}}^2 S_{\text{prop}} \rho}{m} \cdot \delta_T \sin(\alpha+\gamma) \\
b_{12}(\bar{\boldsymbol{x}}) &= \frac{C_M^{\delta_E} Sc\rho}{4\pi eARJm} \cdot V^2 b_1(\bar{\boldsymbol{x}}) \\
b_{13}(\bar{\boldsymbol{x}}) &= \frac{C_M^{\delta_F} Sc\rho}{4\pi eARJm} \cdot V^2 b_1(\bar{\boldsymbol{x}}) \\
b_{21}(\bar{\boldsymbol{x}}) &= \frac{C_{\text{prop}} K_{\text{motor}}^2 S_{\text{prop}} \rho}{m} \cdot \delta_T \cos(\alpha) \\
b_{22}(\bar{\boldsymbol{x}}) &= \frac{C_M^{\delta_E} Sc\rho}{2\pi eARJm} \cdot V^2 b_2(\bar{\boldsymbol{x}}) \\
b_{23}(\bar{\boldsymbol{x}}) &= \frac{C_M^{\delta_F} Sc\rho}{2\pi eARJm} \cdot V^2 b_2(\bar{\boldsymbol{x}})
\end{aligned}
\tag{A.1}
$$

where

$$
\begin{aligned}
b_1(\bar{\boldsymbol{x}}) \triangleq\ & \pi eAR\rho S_{\text{prop}} C_{\text{prop}} \cdot \cos(\alpha+\gamma)\left(K_{\text{motor}}^2 \delta_T^2 - V^2\right) - 2S\rho C_L^{\alpha 2} \cdot \alpha \sin(\gamma) V^2 \\
& + \pi eARS\rho C_L^{\alpha} \cdot \cos(\gamma) V^2 \\
b_2(\bar{\boldsymbol{x}}) \triangleq\ & -0.5\pi eAR\rho S_{\text{prop}} C_{\text{prop}} \cdot \sin(\alpha)\left(K_{\text{motor}}^2 \delta_T^2 - V^2\right) - S\rho C_L^{\alpha 2} \cdot \alpha V^2.
\end{aligned}
$$

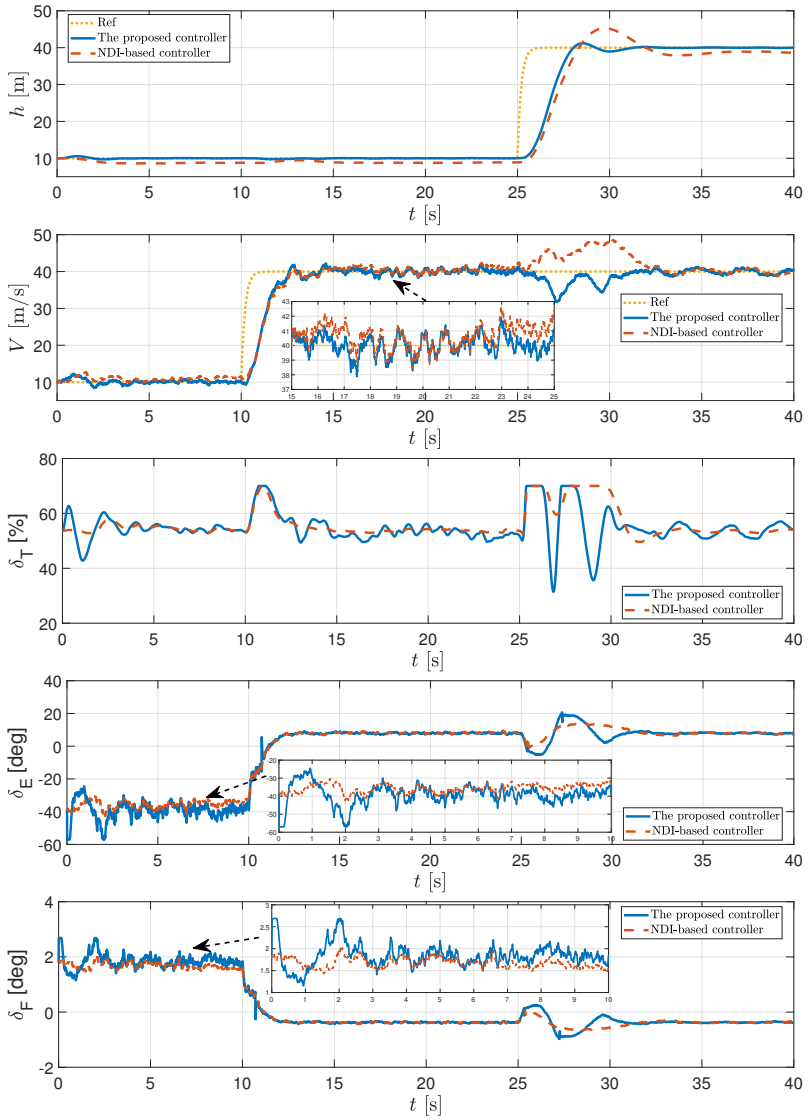

Figure 13: Tracking tests under different control methods.

Appendix B. Parameters of the Aerosonde Aircraft

The detailed coefficients of the Aerosonde aircraft are collected from Table E.2 in [2, Appx. E] and Aerosim blockset [33]. For the convenience of readers, these coefficients are reported in Table B.4.

References

[1] G. Holland, P. Webster, J. Curry, G. Tyrell, D. Gauntlett, G. Brett, J. Becker, R. Hoag, W. Vaglienti, The aerosonde robotic aircraft: A new paradigm for environmental obser-

Table B.4: Aerodynamic coefficients for the Aerosonde UAV

Parameter	Value	Coefficient	Value
m	13.5 [kg]	C_{L0}	0.23
g	9.8 [m/s^2]	C_L^α	5.6106
J	1.135 [kg·m^2]	C_L^q	7.9543
ρ	1.2682 [kg/m^3]	$C_L^{\delta_E}$	0.13
S	0.55 [m^2]	$C_L^{\delta_F}$	0.74
S_{prop}	0.2027 [m^2]	C_{D0}	0.0434
C_{prop}	1	$C_D^{\delta_E}$	0.0135
K_{motor}	80	$C_D^{\delta_F}$	0.1467
e	0.9	C_{M0}	0.135
AR	0.152	C_M^α	-2.7397
c	0.18994 [m]	C_M^q	-38.2067
		$C_M^{\delta_E}$	-0.9918
		$C_M^{\delta_F}$	0.0467

vations, Bulletin of the American meteorological society 82 (5) (2001) 889–902. doi:10.1175/1520-0477(2001)082<0889:TARAAN>2.3.CO;2.

[2] R. W. Beard, T. W. McLain, Small unmanned aircraft: Theory and practice, Princeton university press, 2012.

[3] Q. Hu, G. Niu, C. Wang, Spacecraft attitude fault-tolerant control based on iterative learning observer and control allocation, Aerospace Science and Technology 75 (2018) 245–253. doi:https://doi.org/10.1016/j.ast.2017.12.031.

[4] B. Li, Q. Hu, G. Ma, Y. Yang, Fault-tolerant attitude stabilization incorporating closed-loop control allocation under actuator failure, IEEE Transactions on Aerospace and Electronic Systems 55 (4) (2018) 1989–2000. doi:10.1109/TAES.2018.2880035.

[5] F. Bateman, H. Noura, M. Ouladsine, Fault diagnosis and fault-tolerant control strategy for the Aerosonde UAV, IEEE Transactions on Aerospace and Electronic Systems 47 (3) (2011) 2119–2137. doi:10.1109/TAES.2011.5937287.

[6] R. Jaiswal, A. Shastry, S. Swarnkar, M. Kothari, Adaptive longitudinal control of UAVs with direct lift control, IFAC-PapersOnLine 49 (1) (2016) 296–301. doi:https://doi.org/10.1016/j.ifacol.2016.03.069.

[7] Y. Yan, J. Yang, C. Liu, M. Coombes, S. Li, W.-H. Chen, On the actuator dynamics of dy-

namic control allocation for a small fixed-wing UAV with direct lift control, IEEE Transactions on Control Systems Technology 28 (3) (2020) 984–991. doi:10.1109/TCST.2019.2945909.

[8] M. Niculescu, Lateral track control law for Aerosonde UAV, in: 39th Aerospace Sciences Meeting and Exhibit, 2001, pp. 1–11. doi:10.2514/6.2001-16.

[9] A. Sarhan, M. Ashry, Self-tuned PID controller for the Aerosonde UAV autopilot, International Journal of Engineering Research & Technology (IJERT) 2 (12) (2013) 2278–0181.

[10] R. Socas, S. Dormido, R. Dormido, Event-based control strategy for the guidance of the Aerosonde UAV, in: 2015 European Conference on Mobile Robots (ECMR), 2015, pp. 1–6. doi:10.1109/ECMR.2015.7324213.

[11] P. Poksawat, L. Wang, A. Mohamed, Gain scheduled attitude control of fixed-wing UAV with automatic controller tuning, IEEE Transactions on Control Systems Technology 26 (4) (2017) 1192–1203. doi:https://doi.org/10.1109/TCST.2017.2709274.

[12] T. A. Johansen, T. I. Fossen, Control allocation—A survey, Automatica 49 (5) (2013) 1087–1103. doi:10.1016/j.automatica.2013.01.035.

[13] O. Härkegård, S. T. Glad, Resolving actuator redundancy—Optimal control vs. control allocation, Automatica 41 (1) (2005) 137–144. doi:10.1016/j.automatica.2004.09.007.

[14] X. Lang, A. de Ruiter, A control allocation scheme for spacecraft attitude stabilization based on distributed average consensus, Aerospace Science and Technology 106 (2020) 106173. doi:10.1016/j.ast.2020.106173.

[15] X. Zhang, R. Mu, J. Chen, P. Wu, Hybrid multi-objective control allocation strategy for reusable launch vehicle in re-entry phase, Aerospace Science and Technology (2021). doi:10.1016/j.ast.2021.106825.

[16] O. Härkegård, Dynamic control allocation using constrained quadratic programming, Journal of Guidance, Control, and Dynamics 27 (6) (2004) 1028–1034. doi:10.2514/1.11607.

[17] Q. Hu, B. Li, Y. Zhang, Nonlinear proportional-derivative control incorporating closed-loop control allocation for spacecraft, Journal of Guidance, Control, and Dynamics 37 (3) (2014) 799–812. doi:10.2514/1.61815.

[18] M. W. Oppenheimer, D. B. Doman, Methods for compensating for control allocator and actuator interactions, Journal of Guidance, Control, and Dynamics 27 (5) (2004) 922–927. doi:10.2514/1.7004.

[19] W. A. Kishore, S. Sen, G. Ray, T. K. Ghoshal, Dynamic control allocation for tracking time-varying control demand, Journal of Guidance, Control, and Dynamics 31 (4) (2008) 1150–1157. doi:10.2514/1.34085.

[20] Y. Luo, A. Serrani, S. Yurkovich, M. W. Oppenheimer, D. B. Doman, Model-predictive dynamic control allocation scheme for reentry vehicles, Journal of Guidance, Control, and Dynamics 30 (1) (2007) 100–113. doi:10.2514/1.25473.

[21] M. Hanger, T. A. Johansen, G. K. Mykland, A. Skullestad, Dynamic model predictive control allocation using CVXGEN, in: 2011 9th IEEE International Conference on Control and Automation (ICCA), 2011, pp. 417–422. doi:10.1109/ICCA.2011.6137940.

[22] S. Galeani, A. Serrani, G. Varano, L. Zaccarian, On input allocation-based regulation for linear over-actuated systems, Automatica 52 (2015) 346–354. doi:10.1016/j.automatica.2014.10.112.

[23] T. E. Passenbrunner, M. Sassano, L. Zaccarian, Optimality-based dynamic allocation with nonlinear first-order redundant actuators, European Journal of Control 31 (2016) 33–40. doi:10.1016/j.ejcon.2016.04.002.

[24] M. Furci, C. Nainer, L. Zaccarian, A. Franchi, Input allocation for the propeller-based over-actuated platform rospo, IEEE Transactions on Control Systems Technology 28 (6) (2019) 2720–2727. doi:10.1109/TCST.2019.2944341.

[25] W.-H. Chen, J. Yang, L. Guo, S. Li, Disturbance-observer-based control and related methods—An overview, IEEE Transactions on Industrial Electronics 63 (2) (2015) 1083–1095. doi:10.1109/TIE.2015.2478397.

[26] W.-H. Chen, Nonlinear disturbance observer-enhanced dynamic inversion control of missiles, Journal of Guidance, Control, and Dynamics 26 (1) (2003) 161–166. doi:10.2514/2.5027.

[27] C. Liu, W.-H. Chen, Disturbance rejection flight control for small fixed-wing unmanned aerial vehicles, Journal of Guidance, Control, and Dynamics 39 (12) (2016) 2810–2819. doi:10.2514/1.G001958.

[28] J. Liu, M. Sun, Z. Chen, Q. Sun, Output feedback control for aircraft at high angle of attack based upon fixed-time extended state observer, Aerospace Science and Technology 95 (2019) 105468. doi:https://doi.org/10.1016/j.ast.2019.105468.

[29] T. Manzoor, Z. Sun, Y. Xia, D. Ma, MPC based compound flight control strategy for a ducted fan aircraft, Aerospace Science and Technology 107 (2020) 106264. doi:10.1016/j.ast.2020.106264.

[30] J. Chen, R. Sun, B. Zhu, Disturbance observer-based control for small nonlinear UAV systems with transient performance constraint, Aerospace Science and Technology 105 (2020) 106028. doi:10.1016/j.ast.2020.106028.

[31] R. Sun, Z. Zhou, X. Zhu, Flight quality characteristics and observer-based anti-windup finite-time terminal sliding mode attitude control of aileron-free full-wing configuration uav, Aerospace Science and Technology 112 (2021) 106638. doi:10.1016/j.ast.2021.106638.

[32] A. D. Ames, X. Xu, J. W. Grizzle, P. Tabuada, Control barrier function based quadratic programs for safety critical systems, IEEE Transactions on Automatic Control 62 (8) (2016) 3861–3876. doi:10.1109/TAC.2016.2638961.

[33] U. Dynamics, Aerosim blockset version 1.2 user's guide, Internet: http://www. udynamics. com (2006).

[34] J. T. Parker, A. Serrani, S. Yurkovich, M. A. Bolender, D. B. Doman, Control-oriented modeling of an air-breathing hypersonic vehicle, Journal of Guidance, Control, and Dynamics 30 (3) (2007) 856–869. doi:10.2514/1.27830.

[35] A. Isidori, Nonlinear control systems. communications and control engineering, Springer. 3rd edition. (1995).

[36] Q. Wang, R. F. Stengel, Robust nonlinear control of a hypersonic aircraft, Journal of Guidance, Control, and Dynamics 23 (4) (2000) 577–585. doi:10.2514/2.4580.

[37] M. Lungu, Auto-landing of UAVs with variable centre of mass using the backstepping and dynamic inversion control, Aerospace Science and Technology 103 (2020) 105912. doi:10.1016/j.ast.2020.105912.

[38] G. Wu, X. Meng, Nonlinear disturbance observer based robust backstepping control for a flexible air-breathing hypersonic vehicle, Aerospace Science and Technology 54 (2016) 174–182. doi:https://doi.org/10.1016/j.ast.2016.04.018.

[39] K. P. Tee, S. S. Ge, Control of nonlinear systems with full state constraint using a barrier Lyapunov function, in: Proceedings of the 48h IEEE Conference on Decision and Control (CDC) held jointly with 2009 28th Chinese Control Conference, IEEE, 2009, pp. 8618–8623. doi:10.1109/CDC.2009.5400484.

[40] K. Zhao, Y. Song, Removing the feasibility conditions imposed on tracking control designs for state-constrained strict-feedback systems, IEEE Transactions on Automatic Control 64 (3) (2019) 1265–1272. doi:10.1109/TAC.2018.2845707.

[41] D. Limón, I. Alvarado, T. Alamo, E. F. Camacho, MPC for tracking piecewise constant references for constrained linear systems, Automatica 44 (9) (2008) 2382–2387. doi:10.1016/j.automatica.2008.01.023.

[42] M. Naderi, A. K. Sedigh, T. A. Johansen, Guaranteed feasible control allocation using model predictive control, Control Theory and Technology 17 (3) (2019) 252–264. doi:10.1007/s11768-019-7231-9.

[43] P. Tøndel, T. A. Johansen, A. Bemporad, An algorithm for multi-parametric quadratic programming and explicit MPC solutions, Automatica 39 (3) (2003) 489–497. doi:10.1016/S0005-1098(02)00250-9.

[44] D. J. Moorhouse, R. J. Woodcock, Background information and user guide for MIL-F-8785C, military specification-flying qualities of piloted airplanes, Tech. rep., Air Force Wright Aeronautical Labs Wright-Patterson AFB OH (1982).